ELSEVIER

Colloids and Surfaces
A: Physicochemical and Engineering Aspects 122 (1997) 53–61

COLLOIDS AND SURFACES A

Phase behaviour and long-time self-diffusion in a binary hard sphere dispersion

A. Imhof, J.K.G. Dhont

Van't Hoff Laboratory for Physical and Colloid Chemistry, Utrecht University, Padualaan 8, 3584 CH Utrecht, Netherlands

Received 27 February 1996; accepted 17 August 1996

Abstract

We studied the phase behaviour of, and long-time self-diffusion in, a binary dispersion of hard spheres with a size ratio of 1:9.3. This system exhibits a fluid-crystal-type phase separation. The fluid–solid binodal was determined by measurements of the compositions of coexisting phases, allowing a test of existing theories. By labelling either the large or the small particles with a fluorescent dye the long-time self-diffusion coefficients of both particles could be measured separately using fluorescence recovery after photobleaching (FRAP). Systematic measurements were carried out for a wide range of volume fractions and mixture compositions. The low volume fraction behaviour was compared with existing theory. For higher volume fractions formulae are proposed that represent the data well. At the highest volume fractions long-time self-diffusion becomes arrested when the glass transition is reached. This is evidenced by an incomplete decay of the correlation functions that are measured with FRAP. Evidence was found for the existence of two different glassy states. In one of these both particles are structurally arrested. In the other, however, the small spheres remain mobile, although the large spheres are structurally arrested.

Keywords: Diffusion; Dispersion; Hard spheres; Phase diagram

1. Introduction

Binary hard sphere dispersions have recently attracted much attention as a result of the observation of superlattice formation at the freezing transition [1,2] and phase separation [3–5]. Until now most attention has been focused on the static properties of these asymmetric mixtures and much less is known about their dynamical properties. In this work aspects of both statics and dynamics of a binary colloidal dispersion composed of hard spheres with a size ratio of 1:9.3 are studied. In addition to a study of the phase behaviour, we present a systematic investigation of the long-time self-diffusion coefficient of both the small and the large spheres in the mixtures.

In the description of asymmetric mixtures, the concept of depletion attraction [6,7] is often used. When two large particles approach each other, the smaller particles are expelled from the gap. The difference between the osmotic pressure in the gap and in the bulk induces an effective attraction. An important question is how this affects the phase behaviour. The depletion effect is most clearly seen in mixtures of colloidal hard spheres with polymer molecules. For binary colloids, in which the small particles also behave as hard spheres, the effect is often much less pronounced. So far only parts of the phase diagram have been obtained experimentally, and they differ considerably from one system to another [3–5]. From theoretical studies it seems that the instability depends sensitively on approx-

PII S0927-7757(96)03843-5

imations used for the closure [8–10] or the activity of the small spheres [11,12].

In our mixtures one of the particle species, either the larger or the smaller, is labelled with a fluorescent dye. This enables us to measure the mobility of both particles separately by measuring their long-time self-diffusion coefficients $D_{s,L}$ using the technique fluorescence recovery after photobleaching (FRAP). This also provides information about the nature of the phases formed (fluid, crystal, glass). So far, the study of self-diffusion in dispersions of differently sized particles has mostly been limited to dilute systems of highly charged spheres, in which hydrodynamic interactions are negligible. Since most of the earlier experiments used dynamic light scattering (DLS) to measure particle dynamics, they were limited to dilute dispersions and to the measurement of the larger particles, which scatter most of the light. Few investigations of the long-time self-diffusivity of both particle species exist [13]. Our systematic investigations allow a test of theoretical expressions, given by Batchelor [14], valid up to leading order in the volume fractions of the components. For higher volume fractions we shall present empirical expressions that describe the data well.

2. Experimental details

Colloidal silica particles of two different sizes were prepared, having hydrodynamic radii of 365 and 39 nm [15]. Of both particles we prepared a separate batch in which the cores of the spheres were labelled with the fluorescent dye fluorescein isothiocyanate (FITC) [16], but which were carefully grown to the same size. The unlabelled large particles are called L, and the fluorescent FL. Likewise the small particle systems are called S and FS. All four particles were transferred to a solution of 0.0100 M LiCl in dimethylformamide (DMF). This corresponds to a Debye screening length of only 2.2 nm, making particle interactions essentially hard sphere like. The particles are then stabilized against aggregation by a thin DMF solvation layer of a few nanometres thickness on each particle surface.

Results of the characterization of the four particles are collected in Table 1. SLS was used to measure the size of the large particles. From transmission electron micrographs the polydispersities σ (standard deviation in the radius divided by the mean radius) were determined. DLS was carried out on very dilute samples in DMF (0.01 M LiCl), yielding the particles' diffusion coefficients D_0 at infinite dilution. Hydrodynamic radii were calculated from the D_0 values using the Stokes–Einstein relation.

Effective hydrodynamic volume fractions ϕ of the four dispersions in DMF–0.01 M LiCl were determined by measuring the intrinsic viscosity $[\eta]$. This quantity was determined by measuring the increase in viscosity of dilute dispersions relative to the solvent ($\phi = 0$–0.02):

$$[\eta] = \lim_{\phi \to 0} (\eta/\eta_0 - 1)/\phi \qquad (1)$$

For uncharged spheres $[\eta]$ has the Einstein value of 2.5. The hydrodynamic volume fraction is then calculated by multiplying the dry silica volume fraction, obtained by drying a weighed amount of dispersion, with $[\eta]/2.5$. For the large spheres the factor $[\eta]/2.5$ was about 1.2. For the small particles we found a value of 1.5, reflecting the relatively larger contribution of the solvation layer. All volume fractions ϕ reported in this paper are hydrodynamic volume fractions. The relative error in these values is estimated to be 0.5%.

From concentrated dispersions of L, FL, S, and FS particles, binary mixtures were obtained in which either the small or the large particles are labelled. By varying the ratio ϕ_L/ϕ_S of volume fractions of large and small spheres, phase behaviour was studied in the entire ϕ_L,ϕ_S plane, once with the small spheres labelled and once with the large spheres labelled.

Long-time self-diffusion coefficients $D_{s,L}$ were determined by FRAP, as described in Ref. [17]. In this technique a short pulse of a high intensity laser interference fringe pattern irreversibly bleaches dye molecules inside particles. This creates a long-wavelength sinusoidal pattern of bleached and unbleached particles, which fades away as a result of Brownian motion. The rate of this process is monitored by oscillating the fringes at low intensity over the bleached pattern. The emitted

Table 1
Particle characterization results

Particle	L	FL	S	FS
a(SLS) (nm)	365 ± 5	365 ± 5		
a(DLS) (nm) (DMF[a])	360 ± 10	370 ± 8	39 ± 1	39 ± 1
D_0 ($\times10^{-12}$ m^2 s^{-1}) (DMF[a])		0.739 ± 0.015	6.37 ± 0.18	6.39 ± 0.16
σ	0.03	0.03	0.12	0.12

SLS, static light scattering.
[a] Containing 0.0100 M LiCl.

fluorescence then oscillates as the monitoring and bleached fringes fall into and out of phase, while the amplitude of the oscillation decreases exponentially in time, as exp $(-D_{s,L}k^2t)$ with k the wavevector of the fringes, typically 10^5–10^6 m^{-1}. In each sample, about 15 measurements were recorded and averaged to obtain $D_{s,L}$ with a resulting statistical error of 3% for FS particles and 6% for FL. The larger error in the results of the large spheres is caused by their weaker fluorescence. Diffusion coefficients were normalized with respect to D_0, the value at infinite dilution as measured with DLS (Table 1).

3. Results and discussion

3.1. Phase behaviour

The nature of the different phases is shown in Fig. 1(a). In most of the phase diagram the system is a homogeneous fluid (F). Our phase diagram differs from earlier investigations [3–5] in that we observed a phase separation into a fluid and a crystal formed by the large spheres. This occurred in a region (F+C) in the lower right-hand corner of the diagram, where $\phi_L > \phi_S$. Crystals nucleated homogeneously throughout these samples, giving rise to visible Bragg reflections, and settled under gravity relatively quickly, forming a crystalline sediment. A FRAP signal of the large spheres, measured in the coexisting fluid, is shown in Fig. 2(a). It decays single exponentially to zero, as expected for a fluid. At high volume fractions we could identify two different glassy phases with FRAP. In the first we found that neither of the particle species was fully mobile, and we therefore indicate it by $G_L(G_S)$. The $G_L(G_S)$ phase occurred when $\phi_S > \phi_L$. The long-time self-intermediate scattering function of neither the large nor the small particles exhibited a complete decay: typical examples of FRAP curves are shown in Fig. 2(b). Notice the long time span of the experiments. Samples in this region were very viscous and the speckles in the scattering pattern of the large spheres were static, reflecting their immobility. In the other glass phase, $G_L(F_S)$, only the small particles were free to move. Here, the FRAP curves of the large spheres again decayed only partly, and the scattering speckles were static. At the same time, however, FRAP curves of the small spheres invariably decayed to zero, though in a non-single-exponential way (Fig. 2(c)). The small spheres thus have a complete relaxation. Also, samples in this region appeared to be less viscous than those in the $G_L(G_S)$ phase. Possibly, the small spheres are moving through a kind of porous medium formed by the static large spheres. The two modes in Fig. 2(c) are then explained by a fast intracavity diffusion and a much slower diffusion from one cavity to the next. It is possible that the space-filling large sphere structure of $\phi_L = 0.3$–0.4 is held together by the depletion attraction, caused by the small spheres. However, since evidence for gelation or flocculation is not found at any point in the phase diagram it could also simply be an excluded volume effect. The precise location of the line separating the two glassy states is unknown, if a well-defined transition exists at all.

More information about the fluid–solid coexistence was obtained by constructing the fluid–solid binodal. The binodal consists of a freezing line with fluid phase compositions ($\phi_{f,L}$, $\phi_{f,S}$), and of a melting line with solid phase compositions

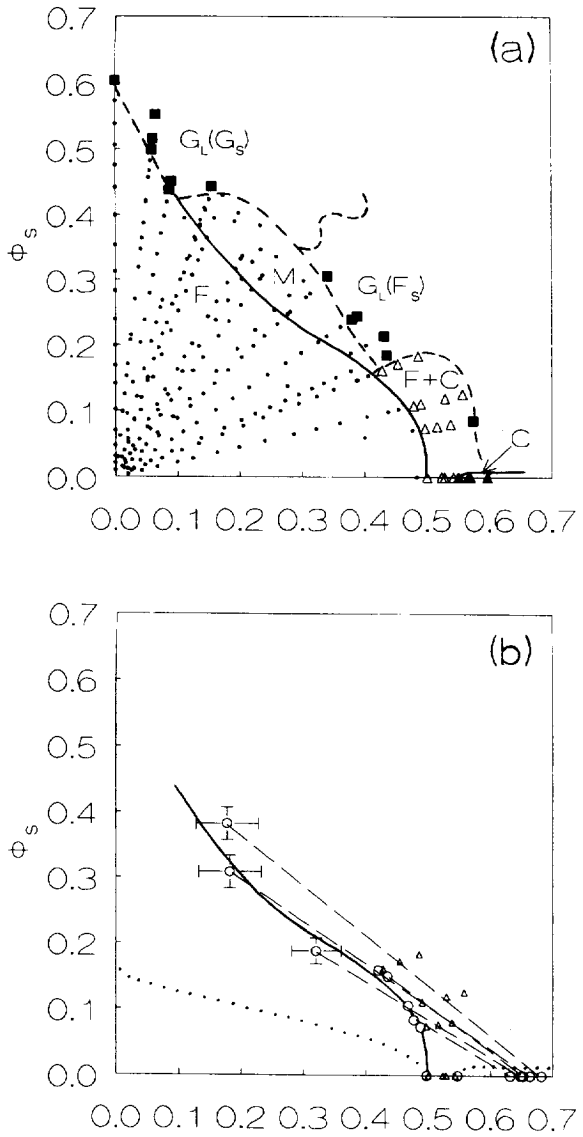

Fig. 1. (a) Phase diagram. ●, homogeneous fluids; ▲, samples separating into fluid and crystal; △, completely crystalline; ■, glassy samples; —, fluid–solid binodal from (b); - - -, glass transition lines. (b) Construction of the fluid–solid binodal (—). ▲, compositions separating into fluid and crystal; - - -, tie lines connecting coexisting compositions (○); ·····, theory from Ref. [12].

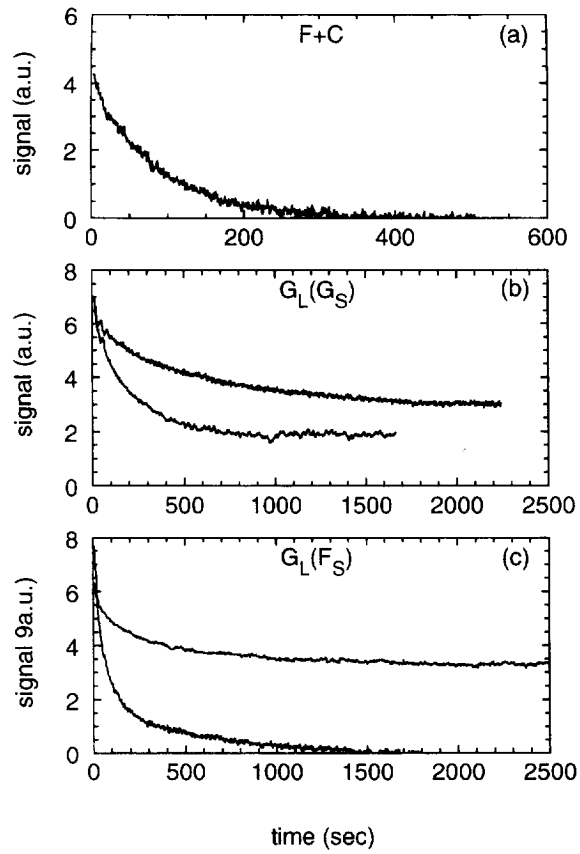

Fig. 2. (a) FRAP signal $S(t)$ of the large spheres measured in the fluid coexisting with the crystal ($\phi_L=0.505$, $\phi_S=0.0910$, $k=780\,240\ m^{-1}$). (b) FRAP signals in the $G_L(G_S)$ phase: large spheres (lower curve, $\phi_L=0.0592$, $\phi_S=0.499$, $k=463\,320\ m^{-1}$); small spheres (upper curve, $\phi_L=0.0609$, $\phi_S=0.516$, $k=206\,060\ m^{-1}$). (c) FRAP signals in the $G_L(F_S)$ phase: large spheres (upper curve, $\phi_L=0.435$, $\phi_S=0.184$, $k=451\,660\ m^{-1}$); small spheres (lower curve, $\phi_L=0.379$, $\phi_S=0.239$, $k=203\,700\ m^{-1}$).

($\phi_{m,L}$, $\phi_{m,S}$). For the one-component large sphere system the freezing and melting volume fractions ϕ_f and ϕ_m were determined in the usual way [18]: the fraction f_{cryst} of the system occupied by the equilibrium crystal phase is found from the height of the sediment after the crystallites have settled. Effects of particle sedimentation and sediment compaction are ruled out by monitoring the subsequent linear growth of the sediment, and extrapolating this to zero time. f_{cryst} increases linearly with the overall volume fraction and extrapolates to zero at ϕ_f, and to unity at ϕ_m. We found $\phi_f=0.497\pm0.004$ and $\phi_m=0.547\pm0.004$, close to the hard sphere reference values of 0.494 and 0.545 [19].

For binary mixtures, points on the freezing and melting lines must be found by determining the

composition of one of the phases. Together with f_{cryst} the composition of the coexisting phase can then be found with the lever rule. The volume fraction of small spheres in the crystal can be taken as zero, since even if the octahedral and tetrahedral sites are filled completely with small spheres, their volume fraction does not exceed 0.01. We determined the volume fraction of large spheres in the crystal from measurements of the Bragg diffraction angle 2θ at the first diffraction maximum. To this end a sample cuvette of 0.2 mm thickness was placed in a cylindrical bath filled with DMF–0.01 M LiCl to avoid refraction at the interface, and illuminated by a laser beam. The Bragg angle was measured while the crystallites were still sedimenting, since otherwise the lattice spacing is reduced by gravitational compaction. Ascribing the diffraction maximum to an f.c.c. (111) reflection the lattice constant b follows from $(2nb \sin\theta/\lambda)^2 = 3$, where n is the solvent refractive index and λ the wavelength in vacuo. The volume fraction $\phi_{m,L}$ of large spheres in the crystal is then $16\pi a_L^3/3b^3$. Although the crystal structure was not determined, it is noted that assuming a hexagonal close packing would lead to exactly the same $\phi_{m,L}$. Since the uncertainty in a_L is 1.4% the error in $\phi_{m,L}$ would be 4%. To avoid making such a large error we calculated $\phi_{m,L}$ by comparing b with the value found in a monodisperse system (1154 nm), so that $\phi_{m,L} = 0.547 \times (1154\ \text{nm}/b)^3$. This no longer depends on a_L and reduces the error to about 1%.

In Fig. 1(b) the resulting fluid–solid binodal is plotted, with coexisting phases connected by tie lines. More points on the freezing line were found by diluting mixtures at constant ϕ_L/ϕ_S to the point where crystallization was no longer observed. Included in the figure is the theoretical binodal from Ref. [12]. Contrary to [3–5], we did not observe fluid–fluid separation. This agrees with recent predictions that the fluid–fluid spinodal is metastable with respect to the fluid–solid binodal [11,12]. The shape of the F+C coexistence region also agrees qualitatively with these theories. However, the latter strongly overestimate the depletion activity of the small spheres. In our system phase separation is found at larger ϕ_S than in Refs. [3–5]. The binodals found in those investigations also differ considerably from each other. Since different particles were used in each case, it could be that the binodal depends sensitively on small deviations from true hard sphere behaviour.

Fig. 1(a) includes the fluid–solid binodal from Fig. 1(b). Although the binodal extends over the full width of the phase diagram, actual crystallization is observed only in a limited region (F+C). Therefore the fluid phases found above part of the binodal are metastable with respect to the fluid–solid binodal (region M). In such systems $D_{s,L}$ of a large sphere was more than 50 times smaller than its value at infinite dilution (Section 3.2.). It is thus not surprising that crystallization rates can be extremely small. Indeed, the time needed for crystallites to become visible increased from about 15 min for monodisperse systems, through several hours for the $\phi_L/\phi_S = 6.696$ mixture, to almost 2 days for $\phi_L/\phi_S = 2.650$.

3.2. Long-time self-diffusion

We shall use the following notation. In the symbol $D_{s,L}^{(i)}$ the subscripts s and L indicate the type of diffusion coefficient (long-time self). In mixtures, the superscript between parentheses refers to the type of particle (small or large) of which the diffusion coefficient is given. If no superscript appears, a one-component system is implied.

For binary mixtures that remained homogeneous, the long-time self-diffusion coefficients of the small (labelled) spheres in the presence of large (unlabelled) spheres are plotted in Fig. 3(a), and for the large (labelled) spheres in the presence of small (unlabelled) spheres in Fig. 3(b). Data of one-component dispersions are also included. The diffusivities are plotted vs. the volume fraction of the labelled species, for several mixture compositions ϕ_L/ϕ_S. Note that, since the data were measured as a series of dilutions at constant ϕ_L/ϕ_S, the volume fraction of unlabelled particles increases in constant proportion to the volume fraction of labelled particles. As expected, all diffusivities decrease monotonically with volume fraction, and more quickly so when the relative amount of unlabelled particles is increased.

Theoretical expressions for mixtures of hard spheres are known only up to the pair interaction level, and are valid up to first order in volume fraction. They were given by Batchelor [14], and

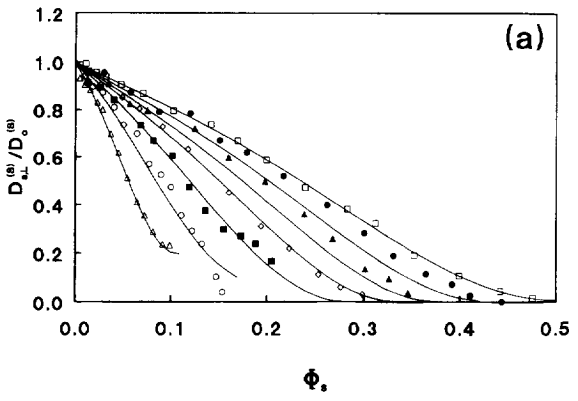

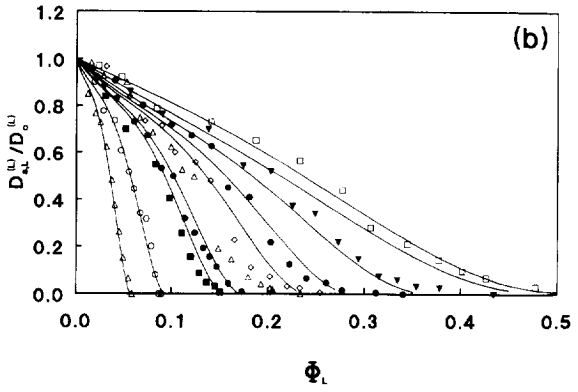

Fig. 3. (a) Long-time self-diffusivities of the small spheres in mixtures of compositions (from left to right curve) $\phi_L/\phi_S = 4.424$, 2.650, 1.588, 1.012, 0.677, 0.349, and only small spheres. (b) Long-time self-diffusivities of the large spheres, with compositions (from left to right curve) $\phi_L/\phi_S = 0.119$, 0.199, 0.356, 0.403, 0.610, 0.775, 1.121, 2.357, and only large spheres. —, results of Eq. (6) and Eq. (7); compositions in the same order.

take into account hydrodynamic interactions. For the present size ratio his results are

$$D_{s,L}^{(S)}/D_0^{(S)} = 1 - 2.10\phi_S - 1.07\phi_L \quad (2a)$$

$$D_{s,L}^{(L)}/D_0^{(L)} = 1 - 2.10\phi_L - 2.38\phi_S \quad (2b)$$

In general the coefficients depend on the particle size ratio and interaction potential. They can be compared with those obtained from the measurements. From Fig. 3 the initial slopes $A^{(i)}$ were obtained, defined by

$$D_{s,L}^{(i)}/D_0^{(i)} = 1 + A^{(i)}\phi_i, \quad i = S,L \quad (3)$$

In terms of Batchelor's theory, Eqs. (2a) and (2b), the quantities $A^{(S)}$ and $A^{(L)}$ depend linearly on the ratios ϕ_L/ϕ_S and ϕ_S/ϕ_L respectively:

$$A^{(i)} = K'_{ii} + K'_{ij}\phi_j/\phi_i \quad (4)$$

The experimental and theoretical $A^{(i)}$ are plotted in Fig. 4. The low volume fraction behaviour of the small spheres follows the theory very well. A weighted least-squares fit gives

$$\frac{D_{s,L}^{(S)}}{D_0^{(S)}} = 1 - \left[(1.97 \pm 0.08) + (1.10 \pm 0.08)\frac{\phi_L}{\phi_S}\right]\phi_S \quad (5a)$$

This should be compared with the theoretical result in Eq. (2a). For the large spheres we also find a

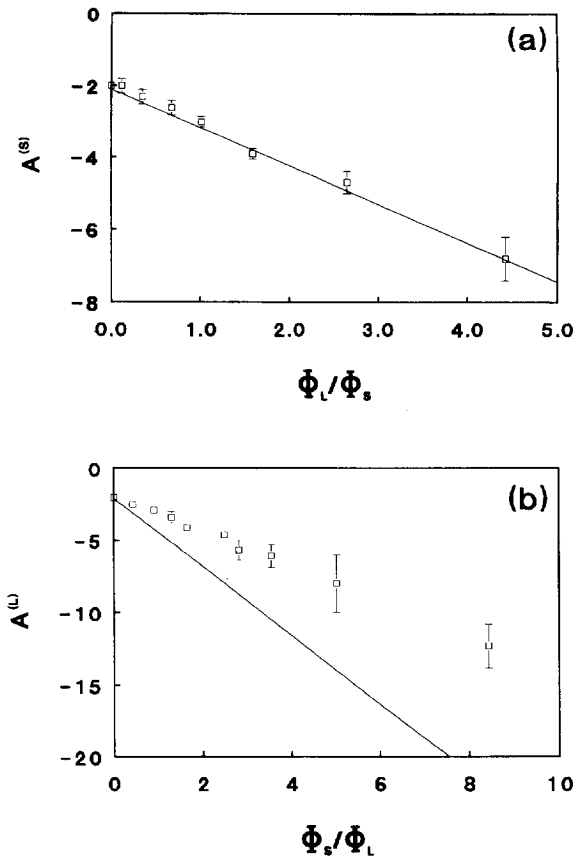

Fig. 4. First order in volume fraction coefficients of $D_{s,L}$ as defined in Eq. (3). (a) Data for small spheres vs. ϕ_L/ϕ_S; (b) data for large spheres vs. ϕ_S/ϕ_L; —, theoretical results from Ref. [14] given in Eqs. (2a) and (2b).

linear result:

$$\frac{D_{s,L}^{(L)}}{D_0^{(L)}} = 1 - \left[(1.96 \pm 0.13) + (1.14 \pm 0.09) \frac{\phi_S}{\phi_L} \right] \phi_L \quad (5b)$$

Comparing with Eq. (2b), it is seen that the intercept in Fig. 4(b), which is determined by L–L interactions, is close to the expected value. However, the slope, determined by L–S interactions, is a factor of 2 smaller than the theory predicts, resulting in a diffusion coefficient that is somewhat larger than expected.

The lack of agreement for the large sphere diffusivity probably has its origin in the huge difference between the numbers of large and small particles. This is a consequence of the extreme difference in the particle volumes of the two species: for all practical values of ϕ_L/ϕ_S the number of small spheres exceeds the number of large spheres by a factor of more than 100. Even in a dispersion as dilute as $\phi_L + \phi_S = 0.01$, a large sphere is therefore unlikely to interact with just one small particle at a time. For this reason the theoretical value $K'_{LS} = -2.38$, which accounts only for pair interactions, is probably not applicable. It is more likely that the measured value $K'_{LS} = -1.14$ corresponds to the friction of a large sphere moving through a dispersion of small spheres, which is in itself dilute in the sense that the small spheres undergo almost exclusively two-particle interactions. It is difficult to estimate how this should influence $D_{s,L}^{(L)}$, because a many-particle theory is not available. The depletion attraction does not provide an explanation for the larger diffusion coefficient found experimentally. Several theories have incorporated the effect of interparticle interactions on $D_{s,L}$ (in addition to the hard core repulsion) up to the pair interaction level. However, they predict that attractions give smaller instead of larger D [14,20].

We now develop a model to describe the diffusivities of both particles in a mixture of any composition. As noted before, a tracer particle, whether it is small or large, interacts much more frequently with small particles than with large particles, since the former are much more abundant and much more mobile (having a larger D_0). Long-range interactions are absent, so between collisions with large particles the tracer effectively diffuses through a dispersion containing only small particles. Therefore, a small tracer particle is interacting most of the time with a neighbouring cage of other small particles, while the large particles are obstacles which it has to diffuse around. A large tracer particle, on the contrary, is so large that it can only be encaged by other large spheres, while the small spheres merely slow down its motion inside the cage. In this view, the interactions between tracer and small spheres are decoupled from the interactions between tracer and large spheres. These considerations led us to a model to describe the $D_{s,L}^{(i)}$ data in a way that is somewhat similar in spirit to an idea of Medina-Noyola [21]. He suggested the separation of $D_{s,L}$ for a one-component system into a factor $D_{s,S}$, accounting for the hydrodynamic interactions that operate on a short time scale, and a factor accounting for collisions between particles that take place on a much longer time scale.

First, imagine that the tracer particle is of the small type, and is placed in a dispersion containing only large spheres. Assume that we know its diffusion coefficient $D_{s,L}^{(S)}(\phi_S \to 0, \phi_L)$ for this situation. Then add many other small spheres up to an overall volume fraction of ϕ_S. Between interactions with the large spheres, the tracer now diffuses through a dispersion of other small spheres with an effective volume fraction of about $\phi_S/(1-\phi_L)$, owing to the excluded volume of the large spheres. Having to move through the dispersion of small spheres reduces the tracer's diffusion coefficient by a factor of $D_{s,L}(\phi_S/(1-\phi_L))/D_0$, which is just the one-component hard sphere value. The resulting diffusion coefficient is then given by

$$D_{s,L}^{(S)}(\phi_S, \phi_L) = D_{s,L}^{(S)}(\phi_S \to 0, \phi_L) \frac{D_{s,L}\left(\dfrac{\phi_S}{(1-\phi_L)}\right)}{D_0} \quad (6)$$

If, on the contrary, the tracer is a large sphere, then its diffusion coefficient, when first placed in a dispersion of other large spheres, is given by the one-component value $D_{s,L}(\phi_L)$. Again small spheres are added. Between collisions with the

large spheres the tracer is slowed down by a factor of $D_{s,L}^{(L)}(\phi_S/(1-\phi_L),\phi_L\rightarrow 0)/D_0^{(L)}$. This is the (relative) diffusion coefficient of a single large sphere in a dispersion of only small spheres. Hence

$$D_{s,L}^{(L)}(\phi_S,\phi_L)=D_{s,L}^{(L)}\left(\frac{\phi_S}{1-\phi_L},\phi_L\rightarrow 0\right)\frac{D_{s,L}(\phi_L)}{D_0} \qquad (7)$$

Eqs. (6) and (7) can be used to predict $D_{s,L}^{(i)}$ in a mixture of any composition, starting from two limiting cases. The second factor on the right-hand sides of Eqs. (6) and (7) is the known one-component quantity, which can be taken from Fig. 3. The first factor in each equation cannot strictly be measured but can be estimated from the mixture with the smallest proportion of respectively small and large spheres. $D_{s,L}^{(S)}(\phi_S\rightarrow 0,\phi_L)$ can thus be obtained from the data in Fig. 3(a) at $\phi_L/\phi_S=4.424$, by dividing it by the second factor in Eq. (6) which is close to unity for this composition. In the same way, the factor $D_{s,L}(\phi_S/(1-\phi_L),\ \phi_L\rightarrow 0)$ follows from the data in Fig. 3(b) at $\phi_L/\phi_S=0.119$ by dividing by the second factor in (7), which is again almost unity.

The predictions of Eqs. (6) and (7) calculated at ϕ_L/ϕ_S ratios corresponding to the experimental ratios are also shown in Fig. 3(a) and 3(b). The small sphere diffusivity is predicted accurately up to high volume fractions. For the large spheres Eq. (7) follows the data well for mixtures with $\phi_L/\phi_S<0.5$. However, for mixtures with a larger proportion of small spheres, $D_{s,L}^{(L)}$ is overestimated considerably at higher volume fractions. This might be an indication that the depletion attraction is active, lowering the diffusivity of the large spheres. However, since the above model ignores multiple interactions of the tracer with two or more particles of different types, this also underestimates the friction on the tracer. It is therefore hard to pinpoint the effect of the depletion attraction on the diffusivity, because there exists no reference in which this attraction is absent.

4. Conclusions

We studied the phase diagram of and long-time self-diffusion in a binary colloidal dispersion with a size ratio of 1:9.3. This mixture exhibits phase separation into a colloidal fluid and a colloidal large sphere crystal. An extended, long-lived metastable fluid region and two different glassy states are also found. In one type of glass state both particle species are structurally arrested. The other glass, occurring in systems that are rich in large spheres, is unusual. Although the large spheres are structurally arrested, the small spheres still exhibit complete relaxation of the FRAP correlation function.

The long-time self-diffusion coefficient of both particle species was extensively studied as a function of composition and total volume fraction. The diffusivity of the small spheres in mixtures with low volume fractions was completely in line with Batchelor's pair interaction theory [14]. The diffusivity of the large spheres in mixtures with small spheres could not be explained by the theory. Because of the large difference in size between the particles, pair interactions between a large sphere and the many small spheres may be so rare that the theory does not apply. For higher volume fractions we proposed Eqs. (6) and (7), in which the friction experienced by a tracer particle due to the presence of the small spheres is decoupled from the friction due to the large spheres. These formulae represent the diffusivities reasonably well for the large spheres, and quite accurately for the small spheres.

References

[1] S. Hachisu and S. Yoshimura, Nature (London), 283 (1980) 188.
[2] P. Bartlett, R.H. Ottewill and P.N. Pusey, J. Chem. Phys., 93 (1990) 1299.
[3] S. Sanyal, N. Easwar, S. Ramaswamy and A.K. Sood, Europhys. Lett., 18 (1992) 107.
[4] J.S. van Duijneveldt, A.W. Heinen and H.N.W. Lekkerkerker, Europhys. Lett., 21 (1993) 369.
[5] P.D. Kaplan, J.L. Rouke, A.G. Yodh and D.J. Pine, Phys. Rev. Lett., 72 (1994) 582.
[6] S. Asakura and F. Oosawa, J. Polym. Sci., 32 (1958) 183.
[7] A. Vrij, Pure Appl. Chem., 48 (1976) 471.
[8] T. Biben and J.P. Hansen, Phys. Rev. Lett., 66 (1991) 2215.
[9] J.J. Lebowitz and J.S. Rowlinson, J. Chem. Phys., 41 (1964) 133.
[10] Y. Rosenfeld, Phys. Rev. Lett., 72 (1994) 3831.

[11] H.N.W. Lekkerkerker and A. Stroobants, Physica A, 195 (1993) 387.
[12] W.C.K. Poon and P.B. Warren, Europhys. Lett., 28 (1994) 513.
[13] X. Qiu, D. Ou-Yang and P.M. Chaikin, J. Phys. France, 49 (1988) 1043.
[14] G.K. Batchelor, J. Fluid Mech., 131 (1983) 155; J. Fluid Mech., 137 (1983) 467 (corrigendum).
[15] W. Stöber, A. Fink and E. Bohn, J. Colloid Interface Sci., 26 (1968) 62.
[16] A. van Blaaderen and A. Vrij, Langmuir, 8 (1992) 2921.
[17] A. Imhof, A. van Blaaderen, G. Maret, J. Mellema and J.K.G. Dhont, J. Chem. Phys., 100 (1994) 2170.
[18] S.E. Paulin and B.J. Ackerson, Phys. Rev. Lett., 64 (1990) 2663.
[19] W.G. Hoover and F.H. Ree, J. Chem. Phys., 49 (1968) 3609.
[20] B. Cichocki and B.U. Felderhof, J. Chem. Phys., 94 (1991) 563.
[21] M. Medina-Noyola, Phys. Rev. Lett., 60 (1988) 2705.